1 **Estimation of bubbled-mediated air/sea gas exchange from**

2 **concurrent DMS and CO$_2$ transfer velocities at**

3 **intermediate-high wind speeds**

4

5 **Thomas G. Bell[1*], Sebastian Landwehr[2], Scott D. Miller[3], Warren J. de Bruyn[4],**

6 **Adrian Callaghan[5], Brian Scanlon[2], Brian Ward[2], Mingxi Yang[1] and Eric S.**

7 **Saltzman[6]**

8 [1] Plymouth Marine Laboratory, Prospect Place, The Hoe, Plymouth, PL1 3DH, UK

9 [2] School of Physics, National University of Ireland, Galway, Ireland

10 [3] Atmospheric Sciences Research Center, State University of New York at Albany, NY, USA

11 [4] Schmid College of Science and Technology, Chapman University, Orange, California, CA, USA

12 [5] Scripps Institution of Oceanography, University of California San Diego, 9500 Gilman Drive, La

13 Jolla, CA 92093

14 [6] Department of Earth System Science, University of California, Irvine, CA, USA

15 *Correspondence to: T.G. Bell (tbe@pml.ac.uk)

16 **Abstract**

17 Simultaneous air/sea fluxes and concentration differences of dimethylsulfide (DMS) and

18 carbon dioxide (CO$_2$) were measured during a summertime North Atlantic cruise in 2011.

19 This dataset reveals significant differences between the gas transfer velocities of these two

20 gases (Δk_w) over a range of wind speeds up to 21 m s^{-1}. These differences occur at and above

21 the approximate wind speed threshold when waves begin breaking. Whitecap fraction (a

22 proxy for bubbles) was also measured and has a positive relationship with Δk_w, consistent

23 with enhanced bubble-mediated transfer of the less soluble CO$_2$ relative to that of the more

24 soluble DMS. However, the correlation of Δk_w with whitecap fraction is no stronger than with

25 wind speed. Models used to estimate bubble-mediated transfer from *in situ* whitecap fraction

26 under-predict the observations, particularly at intermediate wind speeds. Examining the

27 differences between gas transfer velocities of gases with different solubilities is a useful way

28 to detect the impact of bubble-mediated exchange. More simultaneous gas transfer

Atmospheric
Chemistry
and Physics
Discussions

29   measurements of different solubility gases across a wide range of oceanic conditions are

30   needed to understand the factors controlling the magnitude and scaling of bubble-mediated

31   gas exchange.

1   Introduction

33   Air/sea exchange is a significant process for many compounds that have biogeochemical and

34   climatic importance. Approximately 25% of the carbon dioxide (CO_2) released into the

35   atmosphere by anthropogenic activities has been taken up by the world oceans, which has

36   tempered its climate forcing while leading to ocean acidification (Le Quéré et al., 2015). The

37   biogenic gas dimethylsulfide (DMS) is a major contributor to the mass of marine atmospheric

38   aerosol (Virkkula et al., 2006). Volatile organic compounds (VOCs) such as isoprene,

39   acetone and acetaldehyde alter the oxidising capacity of the troposphere (Carpenter et al.,

40   2012). The solubility differences between these VOCs mean that their exchange is controlled

41   to differing degrees by processes on the water and air side of the air/sea interface (Yang et al.,

42   2014). Many of the factors influencing air/sea gas exchange will be altered by future changes

43   in climate, ocean circulation and biology. Earth system models and air quality models require

44   more accurate understanding of the processes that influence air/sea gas transfer.

45   Air/sea gas exchange is typically parameterised as a function of the ocean/atmosphere bulk

46   concentration difference (ΔC) and the physical mixing induced by wind stress at the interface

47   (Liss and Slater, 1974). The air/sea flux is typically described using the expression:

48                        $Flux = K\,(C_w - \alpha C_a)$ *Equation 1*

49   where C_w and C_a are the trace gas bulk concentration on either side of the interface, α is the

50   dimensionless water/air solubility of the gas in seawater and K is the gas transfer velocity.

51   The physics of gas transfer are implicitly represented by the gas transfer velocity, which is

52   commonly expressed in water-side units of velocity (cm hr^{-1}) and parameterized as a function

53   of wind speed (U_{10}) and Schmidt number (Sc). The simplicity of Equation 1 belies the

54   complexity of the processes involved in air/sea gas transfer. These processes include

55   diffusion, surface renewal, buoyancy effects, wave-induced mixing, wave breaking and

56   bubble-mediated transport. A variety of theoretical, laboratory, and field approaches have

57   been used to study these processes but we do not yet have a firm understanding of factors that

58   control air/sea transfer under a range of oceanic conditions.

59   The gas transfer-wind speed relationships for gases of different solubility may be affected by

60   breaking waves and bubbles (Woolf, 1993; Keeling, 1993; Woolf, 1997). Gas transfer via

61   bubbles (k_{bub}) is sensitive to the void fraction (ratio of air volume to total volume) of the

62   bubble plume as well as the bubble size distribution. Bubble injection depth and cleanliness

63   of the surface (influenced by surfactants) affect bubble rise velocity and residence time.

64   Bubble residence time determines the time available for equilibration to occur while bubble

65   volume and gas diffusivity (Sc) govern the time needed for a bubble to equilibrate. The

66   magnitude of k_{bub} is expected to be greater for sparingly soluble gases (e.g. CO_2,

67   dimensionless solubility ~1) than for more soluble gases such as DMS (dimensionless

68   solubility ~15), particularly when bubbles are fully equilibrated.   Bubble-mediated gas

69   transfer has been studied in the laboratory (Rhee et al., 2007; Asher et al., 1996) and using

70   models (e.g. Woolf, 2005; Fairall et al., 2011; Woolf et al., 2007; Goddijn-Murphy et al.,

71   2016).

72   Deliberate, dual-tracer techniques have estimated gas transfer by measuring the evasion of a

73   pair of sparingly soluble gases with different diffusivity (^{3}He and SF_6, dimensionless

74   solubility ≤0.01). These studies indicate non-linear wind speed dependence of the gas transfer

75   velocity, in qualitative agreement with earlier studies in wind-wave tanks (e.g. Watson et al.,

76   1991; Wanninkhof et al., 1985; Liss and Merlivat, 1986). Direct, shipboard measurements of

77   waterside gas transfer have also been made by eddy covariance (e.g. Bell et al., 2013;

78   Marandino et al., 2007; McGillis et al., 2001; Miller et al., 2010; Huebert et al., 2004). These

79   measurements typically show DMS gas transfer velocities that are lower and exhibit more

80   linear wind speed dependence than those estimated for CO_2 based on dual tracer studies (e.g.

81   Bell et al., 2015; Yang et al., 2011; Goddijn-Murphy et al., 2012). It has been suggested that

82   the difference between the open ocean gas transfer velocities of CO_2 and DMS is due to the

83   reduced importance of bubble-mediated exchange for DMS (Goddijn-Murphy et al., 2016;

84   Blomquist et al., 2006; Fairall et al., 2011).

85   Only one set of concurrent CO_2 and DMS gas transfer velocity measurements have been

86   published to date (Miller et al., 2009). In that study, no statistically significant difference was

87   observed in gas transfer-wind speed relationships of CO_2 and DMS for winds below 10 m s^{-1}.

88   This study presents a more extensive set of CO_2 and DMS gas transfer velocities that were

89   measured simultaneously aboard the R/V Knorr in the 2011 summertime North Atlantic in

90   both oligotrophic and highly productive waters. The DMS and CO_2 gas transfer velocities

Atmospheric
Chemistry
and Physics
Discussions

91   are discussed separately in detail by Bell et al. (2013) and Miller et al., In Prep. Here we

92   focus specifically on what can be learned about gas transfer from the differences in behaviour

93   of two different solubility gases at intermediate and high wind speeds.

2   Methods

2.1   Seawater, atmospheric and flux measurement systems

96   The measurement setups for DMS and CO_2 concentrations in air and water and the eddy

97   covariance flux systems have been discussed in detail elsewhere (Bell et al., 2015; Bell et al.,

98   2013; Miller et al., 2010; Miller et al., 2008; Landwehr et al., 2014; Landwehr et al., 2015;

99   Saltzman et al., 2009). We provide a summary and some additional details in the Appendix

100   (Section 6).

2.2   Gas transfer velocity calculations

102   In this section we describe the calculation of DMS and CO_2 gas transfer velocities from the

103   Knorr_11 cruise data. Measured gas transfer velocities are transformed into water side only

104   gas transfer velocities in order to remove the influence of air-side resistance. Air-side

105   resistance is a function of solubility and thus different for the two gases. Finally, we discuss

106   the most appropriate approach for comparing the water-side gas transfer velocities, given that

107   the two gases have different molecular diffusivity and solubility.

108   Total gas transfer velocities (K) are calculated for CO_2 and DMS for each 10-minute flux

109   interval of the Knorr_11 cruise using Equation 1. The temperature-dependent dimensionless

110   solubility of CO_2 and DMS in seawater is calculated following Weiss (1974) and Dacey et al.

111   (1984). These gas transfer velocities reflect the result of resistance on both sides of the

112   interface (Liss and Slater, 1974). The water side contribution to the total resistance is

113   determined as follows:

$$k_w = \left[\frac{1}{K} - \frac{\alpha}{k_a} \right]^{-1} \qquad\qquad \textit{Equation 2}$$

115   where k_w and k_a are the air side and water side gas transfer velocities and α is dimensionless

116   water/air solubility. Note that we use the α reported by Dacey et al. (1984) in these

117   calculations rather than H as there appears to be an error in conversion between α and H in

118   that study (see Supplemental information for discussion). CO_2 solubility is sufficiently low

4

Atmospheric
Chemistry
and Physics
Discussions

119   that air side resistance is negligible and the water side gas transfer is assumed equal to the

120   total transfer velocity ($k_{CO_2} = K_{CO_2}$). The air side resistance for DMS needs to be accounted

121   for because it is a moderately soluble gas (McGillis et al., 2000). Air side gas transfer

122   velocities (k_a) for DMS were calculated for each 10 minute flux interval with the NOAA

123   COAREG 3.1 model, using sea surface temperature (SST) and horizontal wind speed

124   measured during the cruise. The NOAA COAREG 3.1 model (Fairall et al., 2011) is an

125   extension of the COARE bulk parameterization for air/sea energy and momentum fluxes to

126   simulate gas transfer (Fairall et al., 1998; Fairall et al., 2000). The air side gas transfer

127   contributes about 5% on average to the total resistance for DMS. NOAA COAREG 3.1

128   model calculations were carried out using a turbulent/molecular coefficient, A = 1.6, and

129   bubble-mediated coefficient, B = 1.8 (Fairall et al., 2011). Knorr_11 measurements of SST,

130   air temperature, relative humidity, air pressure, downward radiation and wind speed were

131   used as input parameters to the model.

132   To facilitate comparison of transfer coefficients for the two gases across a range of sea

133   surface temperatures, gas transfer velocities are corrected for changes in molecular diffusivity

134   and viscosity. The correction typically involves the normalisation of water side gas transfer

135   velocities to a common Schmidt number (Sc=660), equivalent to CO_2 in seawater at 20°C:

$$k_{X,660} = k_X \cdot \left(\frac{660}{Sc_X}\right)^{-0.5} \qquad\qquad \textit{Equation 3}$$

137   where subscript $_X$ refers to CO_2 or DMS (i.e. $k_{DMS,660}$ and $k_{CO_2,660}$). Temperature-dependent

138   Sc_{CO2} and Sc_{DMS} were obtained using the *in situ* seawater temperature from the ship's bow

139   sensor and parameterisations from Wanninkhof (1992) and Saltzman et al. (1993).

140   The Sc number normalization (Equation 4) is commonly used across the whole range of wind

141   speeds. In fact, it is appropriate only for low or moderate winds in which interfacial gas

142   transfer dominates over bubble-mediated gas exchange. If bubbles are an important

143   component of gas transfer then solubility also plays a role and normalization based on Sc

144   alone may not be sufficient.

145   To develop a more rigorous comparison of k_{DMS} and k_{CO_2}, we normalized the water side

146   transfer velocities of DMS to the Schmidt number of CO_2 at the *in situ* sea surface

147   temperature of each 10-minute flux interval, as follows:

Atmospheric
Chemistry
and Physics
Discussions

148
$$k_{DMS,Sc} = k_{DMS} \cdot \left(\frac{Sc_{CO_2}}{Sc_{DMS}} \right)^{-0.5}$$
Equation 4

149   where Sc_{CO_2} and Sc_{DMS} are the Schmidt numbers of CO_2 and DMS at the *in situ* sea surface

150   temperature. Compared to normalizing both DMS and CO_2 to Sc=660, this approach has the

151   advantage of correcting only k_{DMS}, with no correction to k_{CO2}. The *Sc* correction for DMS

152   should be reasonably accurate, assuming that the bubble-mediated transfer for the more

153   soluble DMS is relatively small.

154   On the Knorr_11 cruise, the variability in sea surface temperature was small ($1\sigma = \pm 1°C$). As

155   a result, there is little difference in the variability or wind speed dependence of *Sc*-corrected

156   k_{CO2} compared to k_{CO2} at the *in situ* temperature (Figure 5 vs. Figure S1 in Supplemental

157   information). In Section 3.4, the relationship between CO_2 and DMS gas transfer velocities

158   and wind speed is examined using $k_{DMS,Sc}$ and kCO_2.

159   ## 2.3   Calculation of k_{bub,CO_2}

160   The water-side controlled gas transfer velocity (k_w) is comprised of interfacial and bubble-

161   mediated transfer mechanisms, which operate in parallel, i.e. $k_w = k_{int} + k_{bub}$ (Woolf, 1997).

162   We assume that turbulence and diffusive mixing at the sea surface operate similarly upon the

163   interfacial air/sea transfer of CO_2 and DMS (i.e. $k_{int,CO2} = k_{int,DMS}$), given appropriate

164   normalization for the differences in molecular diffusivity. Observed differences between

165    $k_{DMS,Sc}$ and k_{CO_2} should therefore be a measure of the difference between the bubble-mediated

166   contributions to DMS and CO_2 gas transfer:

167
$$\Delta k_w = k_{bub,CO_2} - k_{bub,DMS}$$
Equation 5

168   k_{bub,CO_2} and $k_{bub,DMS}$ are related by the influence of solubility and diffusivity upon bubble-

169   mediated transfer. We parameterize this relationship simply as $k_{bub,DMS} = f \cdot k_{bub,CO_2}$.

170   Substitution into Equation 6 yields:

171
$$k_{bub,CO_2} = \frac{\Delta k_w}{1-f}$$
Equation 6

Atmospheric
Chemistry
and Physics
Discussions

Open Access

EGU

172 The value of f depends on seawater temperature and the complex dynamics of bubble

173 formation and cycling (size distributions, surfactants, etc.). At the mean SST encountered in

174 this study (9.8°C), the Woolf (1997) and Asher et al. (2002) bubble gas transfer models yield

175 values for f of 0.14 and 0.27, respectively (see Supplemental information for model

176 equations).

177 **2.4 Sea surface imaging**

178 Whitecap areal fraction was measured using images of the sea surface recorded with a digital

179 camera (5 mega pixel Arecont Vision, 16 mm focal length lens) mounted 14.6 m above the

180 ocean surface at an angle of ~75° from the nadir. Image footprints represent ~7600 m^2 of sea

181 surface. Images were collected at a sample period of about 1 second and post-processed for

182 whitecap fraction according to the Automated Whitecap Extraction algorithm method

183 (Callaghan and White, 2009). Images were further processed to distinguish whitecap pixels

184 as either stage A or stage B whitecaps by applying a spatial separation technique (Scanlon

185 and Ward, 2013). The whitecap fraction measurements were averaged in the same way as the

186 gas transfer velocities (i.e. time-averaged mean values as well as 2 m s^{-1} wind speed bins).

187 **3 Results**

188 **3.1 Cruise location and environmental conditions**

189 This study took place in the summertime North Atlantic (June 24 – July 18, 2011; DOY 175-

190 199), departing and returning to Woods Hole, MA. Most of the data were collected north of

191 50°N, including the occupation of four 24-36 hr stations – ST181, ST184, ST187 and ST191

192 (Figures 1 & 2). The cruise track was designed to sample regions with high biological

193 productivity and phytoplankton blooms, with large air/sea concentration differences for CO_2

194 and DMS. The cruise meteorology and physical oceanography is discussed in detail by (Bell

195 et al., 2013). A series of weather systems travelling from West to East passed over the region

196 during the cruise. Wind speeds ranged from ~1 to 22 m s^{-1}, with strongest winds during the

197 frontal passages at stations ST184 and ST191 (Figure 1b). Atmospheric boundary layer

198 stability was close to neutral for most of the cruise (|z/L| < 0.07; 75% of the time), with

199 infrequent stable conditions (z/L > 0.05; <8% of the time). There was no evidence that the

200 stable periods affected the flux measurements (Bell et al., 2013). Whitecap areal fraction

201 increased up to a maximum of ~0.06 in response to high wind speeds (Figure 1b).

3.2 Whitecaps

202

203 Whitecaps were observed during Knorr_11 when wind speeds exceeded 4.5 m s^{-1}, a typical

204 wind speed threshold for whitecap formation in the open ocean (Schwendeman and

205 Thomson, 2015; Callaghan et al., 2008). Whitecap areal fraction is a strong, non-linear

206 function of wind speed (Figure 3a). The whitecap vs. wind speed relationship for Knorr_11 is

207 similar in shape, but considerably lower than recent previously published wind speed-based

208 whitecap parameterisations (Schwendeman and Thomson, 2015; Callaghan et al., 2008). At

209 intermediate wind speeds the Knorr_11 whitecap data are as much as an order of magnitude

210 lower than the parameterisations (Figure 3a).

211 Total whitecap coverage is a function of (i) active 'stage A whitecaps' (W_A) produced from

212 recent wave breaking and (ii) maturing 'stage B whitecaps' (W_B) that are decaying foam from

213 previous breakers. The Stage A whitecap fraction data is highly variable at ~11 m s^{-1} wind

214 speeds (Figure 3b), which is driven by the difference in the wind-wave conditions during

215 Knorr_11 (ST184 vs ST191, Figure 4a). Stage A whitecap fraction data does not show the

216 same differences between ST184 and ST191 when plotted against the dimensionless

217 Reynolds number, R_H, which describes breaking waves using Knorr_11 measurements of

218 significant wave height (Zhao and Toba, 2001). The relationship between Stage A whitecap

219 fraction and R_H is more scattered when Stage A whitecaps are below ~10^{-4} (Figure 4b). Wave

220 development and steepness (slope) influence the likelihood of breaking waves. Breaking

221 waves are more closely associated with steep, young waves. At a given wind speed and wave

222 height, older, swell-dominated waves do not produce as many stage A whitecaps compared to

223 young wave systems (Callaghan et al., 2008; Sugihara et al., 2007).

3.3 Concentrations, fluxes and gas transfer velocities

224

225 Seawater pCO_2 was consistently lower than the overlying atmosphere throughout the study

226 region due to biological uptake (Figure 1c). As a result, the air/sea concentration difference

227 (ΔpCO_2) was large and always into the ocean, with ΔpCO_2 <-45 ppm for more than 80% of

228 the measurements. Periods with particularly enhanced ΔpCO_2 into the ocean were during the

229 transit between ST181 and ST184 (ΔpCO_2 as large as -120 ppm) and during ST191 (ΔpCO_2

230 consistently -75 ppm).

231   Seawater DMS levels were much higher than atmospheric levels, reflecting the biogenic

232   sources in seawater and the relatively short atmospheric lifetime (~1 day; Kloster et al.,

233   2006). The largest air/sea DMS concentration differences (ΔDMS) of 6-12 ppb were

234   observed during DOY 185-190 (Figure 2a). The ΔDMS and ΔpCO_2 did not co-vary

235   (Spearman $\rho = 0.11$, n=918, $p<0.001$). This is not surprising because, although seawater

236   DMS and CO_2 signals are both influenced by biological activity, they are controlled by

237   different processes. Seawater CO_2 levels reflect the net result of community photosynthesis

238   and respiration, while DMS production is related to metabolic processes that are highly

239   species-dependent (Stefels et al., 2007).

240   CO_2 fluxes (F_{CO2}) were generally into the ocean, as expected given the direction of the air/sea

241   concentration difference (Figure 1d). The variability in F_{CO2} observed on this cruise reflects

242   dependence on both wind speed and ΔpCO_2. For example, during DOY182 air-to-sea CO_2

243   fluxes increase due to a gradual increase in ΔpCO_2 with fairly constant wind speed. More

244   commonly, ΔpCO_2 was fairly constant and variability in F_{CO2} reflected changes in wind

245   speed. For example, from DOY 185-187 wind speeds gradually declined from ~10 to 5 m s^{-1}

246   with a concurrent decline in F_{CO2}. DMS eddy covariance fluxes were always out of the ocean.

247   Ten minute averaged DMS fluxes (F_{DMS}) clearly show the influence of both ΔDMS (e.g.

248   DOY 188) and wind speed (e.g. DOY 184).

249   Gas transfer velocities of CO_2 and DMS from this cruise exhibit two systematic differences:

250   i) k_{DMS} values are generally lower than k_{CO_2}, particularly during episodes of high wind speed;

251   and ii) k_{CO_2} is characterized by much larger scatter than k_{DMS}. We attribute the large scatter in

252   k_{CO_2} to the greater random uncertainty associated with the eddy covariance measurement of

253   air/sea CO_2 fluxes compared to those of DMS. As shown by Miller et al. (2010), the

254   analytical approach used in this study (dried air, closed path LI7500) has sufficient precision

255   to adequately resolve the turbulent fluctuations in pCO_2 associated with the surface flux over

256   most of the cruise ($\Delta pCO_2 < -30$ ppm). The scatter in the CO_2 flux measurements is more

257   likely due to environmental variability resulting from fluctuations in boundary layer CO_2

258   mixing ratio arising from horizontal and/or vertical transport unrelated to air/sea flux (Edson

259   et al., 2008; Blomquist et al., 2014). These effects likely have a much smaller effect on

260   air/sea DMS fluxes, because the air/sea DMS concentration difference is always much larger

261   than the mean atmospheric DMS concentration (due to the short atmospheric lifetime of

Atmospheric
Chemistry
and Physics
Discussions

262   DMS). For example, a ΔpCO_2 of 100 ppm at a wind speed of 10 m s^{-1} will produce turbulent

263   fluctuations that are ~0.02% of the background CO_2 on average. In contrast, a typical

264   seawater DMS concentration (2.6 nM) at 6 m s^{-1} generates fluctuations of 20% of the

265   background (Table 1; Blomquist et al., 2012). Thus, F_{CO2} measurements are highly sensitive

266   to small fluctuations in background CO_2 and the relative uncertainty is expected to be much

267   larger than that for F_{DMS}.

268   ### 3.4   Comparison of k_{CO_2} and $k_{DMS,Sc}$

269   The differences between CO_2 and DMS gas transfer velocities observed in the time series are

270   also evident when the data are examined as a function of wind speed. From the 10-minute

271   averaged data, it is clear that k_{CO_2} is greater than k_{DMS} and has a stronger wind speed-

272   dependence over most of the wind speed range (Figure 5a,b). These broad trends are also

273   easily seen in longer time-averaged data. Flux and ΔC measurements were averaged into 4

274   hour periods (minimum of 3 flux intervals per 4 hour period), which reduced the scatter in

275   F_{CO2} while preserving the temporal variability (Figure S3). Gas transfer velocities were then

276   recalculated from the 4 hour averaged data. 10-minute k_{CO_2} and $k_{DMS,Sc}$ data were also

277   averaged into 2 m s^{-1} wind speed bins, with a minimum of 5 ten minute periods per bin. The 4

278   hour averaged data and the wind speed binned data show k_{CO_2} and $k_{DMS,Sc}$ diverging at

279   intermediate wind speeds, differing by a factor of roughly two at 10 m s^{-1} (Figure 5c,d).

280   DMS gas transfer velocities on this cruise exhibit complex behaviour at intermediate to high

281   wind speeds, as discussed in Bell et al. (2013). $k_{DMS,Sc}$ increases linearly with wind speed up

282   to ~11 m s^{-1} (Figure 5). Under the high wind, high wave conditions encountered during

283   ST191, the wind speed-dependence of $k_{DMS,Sc}$ was lower than expected, with a slope roughly

284   half that of the rest of the cruise data. This effect was not observed at ST184. Such coherent

285   spatial-temporal variation means that wind speed bin averaging of the higher wind speed

286    $k_{DMS,Sc}$ may mask real variability in the relationship with wind speed. Relationships

287   developed from wind speed bin-averaged gas transfer data should be interpreted with caution,

288   especially when it comes to developing generalizable air/sea gas transfer models.

289   The Knorr_11 k_{CO_2} data also demonstrate a clear wind speed dependence (Figure 5). The

290   NOAA COARE model for CO_2 has been tuned to previous eddy covariance flux

291   measurements (McGillis et al., 2001), with bubble-mediated transfer determining the non-

292   linear relationship with wind speed (Fairall et al., 2011). There is reasonable agreement

293   between the COARE model gas transfer velocity predictions and the Knorr_11 k_{CO_2} data

294   until ~11 m s^{-1} wind speed. Above 11 m s^{-1}, the COARE model over predicts k_{CO_2}. This

295   could be interpreted as indicating high wind speed suppression of gas transfer for CO_2 as

296   observed for DMS (as discussed by Bell et al., 2013). However, it is important to note that

297   the number of high wind speed (>15 m s^{-1}) gas transfer measurements in this study is limited

298   to 9 hours and 16 hours of data for DMS and CO2 respectively. Much more data are needed

299   in order to firmly establish the high wind speed behaviour.

300   The COAREG 3.1 model parameterizes interfacial gas transfer by scaling to Sc and friction

301   velocity and estimates bubble-mediated gas transfer following Woolf (1997). The lower

302   solubility of CO_2 leads to enhanced gas transfer relative to that of DMS at high wind speeds

303   where bubble transport is significant (Fairall et al., 2011). There is good agreement between

304   the COAREG model gas transfer velocity predictions and the Knorr_11 k_{CO_2} and k_{DMS} data

305   until ~11 m s^{-1} wind speed.

306   Earlier in this paper we introduced the quantity Δk_w as an observational measure of the

307   difference in gas transfer velocities of CO_2 and DMS (Section 2.3, equation 6). The

308   relationship between Δk_w and wind speed is positive and shows no systematic differences

309   related to temporal variability (Figure 6). Sea surface temperature (SST) is indicated by

310   symbol size. Some of the scatter in Figure 6 could be driven by changes in Sc due to SST

311   variability. Nearly all of the data in Figure 6 is from periods when SST was relatively

312   constant (9.8±1.0°C). Many of the k_{CO_2} data with warm seawater (i.e. ST181, SST > 12°C)

313   were rejected by our quality control criteria (see Section 6.3). These data were collected when

314   wind speeds were low, which resulted in small CO_2 fluxes with large variability at low

315   frequencies. Of the periods with SST > 12°C that passed the quality control criteria, the

316   majority contributed fewer data within a 4 hour averaging period than the minimum threshold

317   (three 10 minute averaged data points). Only one 4 hour period passed the thresholds for flux

318   quality control and number of points, and this was associated with the most negative Δk_w

319   value.

Atmospheric
Chemistry
and Physics
Discussions

Open Access

EGU

4 Discussion

The bubble-mediated component of gas transfer is a strong function of wind speed and breaking waves. Previous estimates of bubble-mediated air/sea gas exchange have been based on laboratory experiments (Asher et al., 1996; Woolf, 1997; Keeling, 1993). The differences between gas transfer velocities for DMS and CO_2 provide a unique way to constrain the importance of bubble-mediated transfer under natural conditions. This study shows that Δk_w is near zero at very low wind speeds ($U_{10} \leq 4.5$ m s^{-1}), which is consistent with the wind speed at which whitecap fraction becomes significant ($> 10^{-5}$, Figure 3a). Above 4.5 m s^{-1}, Δk_w increases non-linearly, consistent with an increase in bubble-mediated CO_2 transfer associated with wave breaking. The relationship between Δk_w and wind speed is non-linear, and the quadratic wind speed-dependence yields a good fit ($R^2 = 0.77$; Figure 6):

$$\Delta k_w = 0.157 U_{10}^2 - 0.535 U_{10} + 4.289 \qquad \textit{Equation 7}$$

The functional form of this relationship is qualitatively consistent with those found between U_{10} and breaking waves/wave energy dissipation (Melville and Matusov, 2002) and U_{10} vs. whitecap areal fraction (e.g. Callaghan et al., 2008; Schwendeman and Thomson, 2015). Bubble-mediated gas transfer is the only viable explanation for the magnitude and wind-speed dependence of Δk_w. The only alternative explanation would require a large systematic bias in the measurement of relative gas transfer velocities of DMS and CO_2. There are no obvious candidates for such biases.

During strong wind/large wave conditions, the Knorr_11 data suggest that bubble-mediated exchange is a dominant contributor to the total transfer of CO_2. For example, when wind speeds were 11-12 m s^{-1}, Δk_w was about 50% of the total CO_2 gas transfer (k_{CO_2}). A significant contribution by bubbles to the total gas transfer velocity means that bubble-mediated exchange must be included and adequately parameterised by gas transfer models. The Schmidt number (Sc) normalisation (Equation 4) assumes that the gas transfer velocity is purely interfacial. An alternative normalisation (involving Sc and solubility) is required when bubble-mediated transfer is significant. Our data suggest that the current Sc normalisation should be applied with caution to gas transfer data for different solubility gases at wind speeds greater than 10 m s^{-1}.

If Δk_w reflects the difference between the bubble-mediated contribution to the transfer of CO_2 and DMS, one would expect Δk_w to correlate with wave-breaking, and hence with the areal

Atmospheric
Chemistry
and Physics
Discussions

351 coverage of whitecaps. Breaking waves generate plumes of bubbles (Stage A whitecaps,

352 W_A), which then rise to the surface and persist for a short period as foam (Stage B whitecaps,

353 W_B). Almost all whitecap measurements represent the fraction of the sea surface that is

354 covered by bubble plumes and/or foam i.e. $W_T = W_A + W_B$. Δk_w is positively correlated with

355 both W_T (Spearman $\rho = 0.81$, n=32, $p<0.001$) and W_A (Spearman $\rho = 0.82$, n=26, $p<0.001$)

356 (Figure 7a,b). These correlations are approximately the same strength as the correlation

357 between Δk_w and wind speed (Spearman $\rho = 0.83$, n=55, $p<0.001$). The functional form of the

358 relationship between Δk_w and whitecap areal extent appears to be linear. However, the

359 Knorr_11 dataset is small and quite scattered. More data are required to fully test the validity

360 of whitecap areal fraction as a proxy for bubbles and bubble-mediated exchange.

361 Observations of the decaying white cap signal (W_B) suggest that the persistence of surface

362 foam is related to sea surface chemistry (Callaghan et al., 2013). W_B is approximately an

363 order of magnitude larger than W_A and thus dominates the W_T signal. It is often assumed that

364 gas exchange takes place in bubble plumes formed by active wave breaking (i.e. W_A), while

365 W_B may vary widely due to surfactant concentration with little or no impact upon bubble-

366 mediated gas exchange (e.g. Pereira et al., 2016). In this case, Δk_w should be more strongly

367 correlated with W_A than W_B or W_T. The Knorr_11 data do not suggest that W_A is an

368 improvement upon either W_T or even wind speed as a measure of bubble mediated exchange.

369 This may be because whitecaps do not fully represent the bubbles facilitating gas exchange as

370 these may dissolve before they reach the sea surface. Alternatively, W_T and W_A may be

371 equally good (or poor) proxies for bubbles because: (i) surfactant activity was minimal in the

372 study region (despite high biological productivity) such that W_B does not confound the

373 relationship between W_T and W_A; (ii) W_A is no better than W_T at representing the volume of air

374 entrained by breaking waves; and/or (iii) bubbles residing at the surface (i.e. W_B) continue to

375 contribute to gas transfer (Goddijn-Murphy et al., 2016).

376 As shown earlier, the bubble-mediated contribution to gas transfer (k_{bub,CO_2}) can be obtained

377 from Δk_w using information from mechanistic bubble gas transfer models (f, see Section 2.3).

378 The k_{bub,CO_2} datasets derived from the Knorr_11 data using the Asher et al. (2002) and Woolf

379 (1997) models differ by about 15% (Figure 8). The field-based estimates of k_{bub,CO_2} can also

380 be compared to model-only estimates for the Knorr_11 conditions using the Asher et al.

381 (2002) and Woolf (1997) models. Both models are based on whitecap areal fraction, W_T. A

Atmospheric
Chemistry
and Physics
Discussions

Open Access

EGU

382   non-linear fit of the Knorr_11 W_T and wind speed measurements ($W_T = 1.9 \times 10^{-6} U_{10n}^{3.36}$) was

383   used to drive both models (Figure 8). Asher et al. (2002) is based on laboratory tipping

384   bucket gas evasion experiments (Asher and Wanninkhof, 1998) and the model was then

385   adjusted to represent the flux of CO_2 into the ocean (invasion). Woolf (1997) scaled a single

386   bubble model to the open ocean based on laboratory experiments.

387   Both models significantly underestimate k_{bub,CO_2} at wind speeds below about 11 m s^{-1}. At

388   higher wind speeds, the Asher et al. (2002) model increases rapidly with wind speed to agree

389   slightly better with the Knorr_11 data. In contrast, Woolf (1997) consistently underestimates

390   k_{bub,CO_2} at all wind speeds. A 'dense plume model' was also developed by Woolf et al. (2007)

391   to take account of the interaction of a bubble plume with the interstitial water between

392   bubbles. This model yields estimates of k_{bub,CO_2} that are even lower than the original Woolf

393   (1997) 'single bubble model' (data not shown).

394   It is likely that the Knorr_11 cruise data will be compared with estimates of k_{bub,CO_2} derived

395   from future field campaigns, which will be conducted under different environmental

396   conditions. Our k_{bub,CO_2} data is at *in situ* seawater temperature (~10°C) and thus *in situ* CO_2

397   solubility (α=1.03) and diffusivity (Sc=1150). We use the Asher et al. (2002) and Woolf

398   (1997) bubble models to make estimates of k_{bub,CO_2} normalised to a standard seawater

399   temperature of 20°C ($k_{bub,CO_2,20°C}$, where α=0.78 and Sc=666). The 4 hour averaged Knorr_11

400   cruise data, including estimates of Δk_w, k_{bub,CO_2} and $k_{bub,CO_2,20°C}$, are provided in Supplemental

401   Table S1.

402   The approach used in this study to estimate Δk_w and k_{bub,CO_2} from the Knorr_11 field data

403   neglect the effect of sea surface skin temperature and CO_2 chemical enhancement. Skin

404   temperature is typically only a few tenths of a degree less than bulk seawater under the

405   conditions encountered in this study (Fairall et al., 1996). The impact upon k_{CO_2} due to skin

406   temperature effects on CO_2 solubility and carbonate speciation is likely on the order of 3%

407   (Woolf et al., 2016). There is a chemical enhancement of the CO_2 flux due to ionization at

408   the sea surface (Hoover and Berkshire, 1969). The effect on k_{CO_2} has been estimated to be up

409   to about 8% at a wind speed of 4-6 m s^{-1} (Wanninkhof and Knox, 1996), which amounts to a

410   maximum impact of a few cm hr^{-1}. By neglecting these effects we have slightly

411   overestimated Δk_w and k_{bub,CO_2}, but the magnitude of these corrections would be small relative

412   to the environmental scatter or measurement uncertainty.

5   Conclusions

414   The Knorr_11 concurrent measurements of DMS and CO_2 gas transfer velocities show

415   significant differences in gas transfer between the two gases at intermediate-high wind

416   speeds. These data indicate that: i) bubble-mediated gas transfer becomes significant for CO_2

417   at or above the threshold for wave-breaking; and ii) the wind speed-dependence is non-linear,

418   with a similar functional form to proposed relationships predicting whitecap areal extent from

419   wind speed. However, existing models of bubble-mediated gas transfer using the Knorr_11 *in*

420   *situ* observations of whitecap fraction significantly underestimate the importance of this

421   process.

422   There are a number of assumptions behind model estimates of bubble-mediated gas exchange

423   (Goddijn-Murphy et al., 2016). Model bias can be crudely split into: i) uncertainties in the

424   scaling of whitecap fraction to the bubble population (e.g. using Cipriano and Blanchard,

425   1981); and ii) the relationship between gas exchange and bubble properties, which are

426   predicted as a function of air entrainment into the surface ocean by a breaking wave, bubble

427   injection depth, size distribution and mobility through the water (a function of surface

428   cleanliness and surfactants). The underestimation of bubble-mediated CO_2 gas transfer by

429   both models is particularly apparent at low-intermediate wind speeds and low whitecap

430   fraction. This could indicate that either bubble production during microscale breaking is an

431   important process for gas transfer or the relationship between whitecap fraction and the

432   bubble population is poorly constrained.

433   In summary, the approach of using simultaneous measurements of multiple gases with

434   different solubility appears to be a viable way to constrain the magnitude of bubble-mediated

435   gas transfer. Analysis of additional sparingly soluble gases, such as methane or oxygenated

436   hydrocarbons would further strengthen this approach. A much larger data set, under a wider

437   range of oceanographic conditions is certainly needed. In particular, it would be useful to

438   examine DMS and CO_2 gas transfer velocities in ocean regions with different temperatures,

439   where the solubility of each gas is significantly different from this study.

440

Atmospheric
Chemistry
and Physics
Discussions

Appendix A

A.1 Seawater CO_2 and DMS measurements

Seawater CO_2 and DMS were monitored in the supply of seawater pumped continuously through the ship from an intake on the bow located 6 m below the sea surface. CO_2 was equilibrated with air in a recirculating showerhead-type system. Alternate air and water side pCO_2 were each measured for 5 min by the same Infrared Gas Analyser (IRGA). Seawater DMS was equilibrated with DMS-free air in a tubular porous membrane equilibrator, operated in a single-pass, counterflow mode. DMS was measured at 1 Hz using chemical ionization mass spectrometry and bin-averaged at 1 minute intervals (UCI miniCIMS; Saltzman et al., 2009). DMS was calibrated by continuously pumping an internal standard of tri-deuterated, DMS (d3-DMS) into the seawater flow just before the equilibrator. Details of the methods and instrumentation used for equilibration and detection of seawater DMS are described in Saltzman et al. (2009).

A.2 Mast-mounted instrumentation and data acquisition

The eddy covariance setup was mounted 13.6 m above the sea surface on the bow mast. Platform angular rates and accelerations were measured by two Systron Donner Motion Pak II (MPII) units. Three dimensional winds and sonic temperature were measured by two Campbell CSAT3 sonic anemometers. Air sampling inlets for DMS and CO_2 were located at the same height as the anemometers and within 20 cm of the measurement region. GPS and digital compass output were digitally logged at 1 Hz. Winds were corrected for ship motion and orientation as described in Miller et al. (2008) and Landwehr et al. (2015). The eddy covariance data streams were logged in both analog and digital format as described in Bell et al. (2013) and Miller et al., In Prep.

A.3 High frequency atmospheric DMS and CO_2 measurements

Atmospheric DMS measurements were made at 10 Hz using an atmospheric pressure chemical ionisation mass spectrometer located in a lab van (UCI mesoCIMS; Bell et al. (2013)). Air was drawn to the instrument through a 28 m long ½ in OD Teflon tube. A subsample of the air stream was passed through a Nafion drier prior to entering the mass

469   spectrometer.   The measurement was calibrated using an internal gas standard of tri-

470   deuterated DMS added to the inlet (see Bell et al., 2013).

471   Atmospheric CO_2 measurements were made on air drawn at 8 L min^{-1} through a filtered inlet

472   (90 mm diameter with 1 micron pore size, Savillex) near the sonic anemometers on the bow

473   mast, through 5 m of 5.9 mm ID polyethylene-lined Dekabon tubing to two fast-response

474   CO_2/H_2O IRGAs in an enclosure on the bow mast. The IRGAs were open-path style sensors

475   (LI7500, Licor Inc.) converted to a closed-path configuration (see Miller et al., 2010) and

476   were plumbed in series. A Nafion multi-tube membrane drier (PD-200T, PermaPure) with 6

477   L min^{-1} dry air counter flow was installed between the two IRGAs such that the upstream

478   IRGA sampled undried air and the downstream IRGA sampled the same air after drying. This

479   technique removes 97% of the Webb Correction from the measured CO_2 flux (first shown by

480   Miller et al. (2010) and confirmed by Landwehr et al. (2014)).

481   The air flow through both the CO_2 and DMS inlets was fully turbulent (Re > 10,000). The

482   inlets used in this study introduced a small delay (Δt = 2.2 s for DMS, Δt = 1.2 s for CO_2)

483   between measured wind and atmospheric measurements, as well as minor loss of covariance

484   at high frequencies (<5%). The methods used to estimate the delay and loss of flux are given

485   in Bell et al. (2013).

486   Eddy covariance fluxes were computed for DMS and CO_2 as F_{DMS} or $F_{CO2} = \sigma_{air} \langle w'c' \rangle$

487   where σ_{air} is the dry air density, w' is the fluctuation in vertical winds and c' is the delay-

488   adjusted fluctuation in gas concentration. Average covariance fluxes were processed in 10

489   minute and 9.5 minute intervals for DMS and CO_2, respectively (hereafter referred to as 10

490   minute intervals). Momentum and sensible heat fluxes were also computed for 10 minute

491   intervals (see Bell et al., 2013).

492   Sampling intervals with a mean wind direction relative to the bow of >90° were excluded

493   from the final data set. CO_2 fluxes were also excluded from intervals when either: i) relative

494   wind direction changed excessively (SD > 10°); ii) relative wind speed was low (< 1 m s^{-1});

495   or iii) ΔCO_2 was low (< |30| ppm). DMS and CO_2 fluxes were quality controlled for excessive

496   low frequency flux as described in the Supplemental information of Bell et al. (2013). These

497   quality control criteria excluded 62% of the intervals for CO_2 and 55% for DMS and

498   significantly reduced the scatter in the data.

499

Atmospheric
Chemistry
and Physics
Discussions

Open Access

EGU

507

508   **References**

509   Asher, W., Edson, J., McGillis, W., Wanninkhof, R., Ho, D. T., and Litchendor, T.: Fractional area whitecap
510   coverage and air-sea gas transfer velocities measured during GasEx-98, in: Gas Transfer at Water Surfaces,
511   American Geophysical Union, 199-203, 2002.

512   Asher, W. E., Karle, L. M., Higgins, B. J., Farley, P. J., Monahan, E. C., and Leifer, I. S.: The influence of
513   bubble plumes on air-seawater gas transfer velocities, J Geophys Res-Oceans, 101, 12027-12041, 1996.

514   Asher, W. E., and Wanninkhof, R.: The effect of bubble-mediated gas transfer on purposeful dual-gaseous tracer
515   experiments, Journal of Geophysical Research: Oceans, 103, 10555-10560, 10.1029/98jc00245, 1998.

516   Bell, T. G., De Bruyn, W., Miller, S. D., Ward, B., Christensen, K., and Saltzman, E. S.: Air/sea DMS gas
517   transfer in the North Atlantic: evidence for limited interfacial gas exchange at high wind speed, Atm Chem
518   Phys, 13, 11073-11087, 2013.

519   Bell, T. G., De Bruyn, W., Marandino, C. A., Miller, S. D., Law, C. S., Smith, M. J., and Saltzman, E. S.:
520   Dimethylsulfide gas transfer coefficients from algal blooms in the Southern Ocean, Atm Chem Phys, 15, 1783-
521   1794, 10.5194/acp-15-1783-2015, 2015.

522   Blomquist, B. W., Fairall, C. W., Huebert, B. J., Kieber, D. J., and Westby, G. R.: DMS sea-air transfer
523   velocity: Direct measurements by eddy covariance and parameterization based on the NOAA/COARE gas
524   transfer model, Geophysical Research Letters, 33, art. no.-L07601, 10.1029/2006gl025735, 2006.

525   Blomquist, B. W., Fairall, C. W., Huebert, B. J., and Wilson, S. T.: Direct measurement of the oceanic carbon
526   monoxide flux by eddy correlation, Atmos Meas Tech, 5, 3069-3075, 10.5194/amt-5-3069-2012, 2012.

527   Blomquist, B. W., Huebert, B. J., Fairall, C. W., Bariteau, L., Edson, J. B., Hare, J. E., and McGillis, W. R.:
528   Advances in air-sea CO_2 flux measurement by eddy correlation, Boundary-Layer Meteorology, 152, 245-276,
529   10.1007/s10546-014-9926-2, 2014.

530   Callaghan, A. H., de Leeuw, G., Cohen, L., and O'Dowd, C. D.: Relationship of oceanic whitecap coverage to
531   wind speed and wind history, Geophysical Research Letters, 35, n/a-n/a, 10.1029/2008gl036165, 2008.

532   Callaghan, A. H., and White, M.: Automated processing of sea surface images for the determination of whitecap
533   coverage, Journal of Atmospheric and Oceanic Technology, 26, 383-394, 10.1175/2008jtecho634.1, 2009.

534   Callaghan, A. H., Deane, G. B., and Stokes, M. D.: Two regimes of laboratory whitecap foam decay: Bubble-
535   plume controlled and surfactant stabilized, Journal of Physical Oceanography, 43, 1114-1126, 10.1175/Jpo-D-
536   12-0148.1, 2013.

537   Carpenter, L. J., Archer, S. D., and Beale, R.: Ocean-atmosphere trace gas exchange, Chem Soc Rev, 41, 6473-
538   6506, 10.1039/c2cs35121h, 2012.

539   Cipriano, R. J., and Blanchard, D. C.: Bubble and aerosol spectra produced by a laboratory 'breaking wave',
540   Journal of Geophysical Research: Oceans, 86, 8085-8092, 10.1029/JC086iC09p08085, 1981.

541 Dacey, J. W. H., Wakeham, S. G., and Howes, B. L.: Henry's law constants for dimethylsulfide in fresh water
542 and seawater, Geophysical Research Letters, 11, 991-994, 1984.

543 Edson, J. B., DeGrandpre, M. D., Frew, N. M., and McGillis, W. R.: Investigations of air-sea gas exchange in
544 the CoOP Coastal Air-Sea Chemical Exchange Project, Oceanography, 21, 34-45,
545 http://dx.doi.org/10.5670/oceanog.2008.03, 2008.

546 Fairall, C. W., Bradley, E. F., Godfrey, J. S., Wick, G. A., Edson, J. B., and Young, G. S.: Cool-skin and warm-
547 layer effects on sea surface temperature, J Geophys Res-Oceans, 101, 1295-1308, 10.1029/95jc03190, 1996.

548 Fairall, C. W., Yang, M., Bariteau, L., Edson, J. B., Helmig, D., McGillis, W., Pezoa, S., Hare, J. E., Huebert,
549 B., and Blomquist, B.: Implementation of the Coupled Ocean-Atmosphere Response Experiment flux algorithm
550 with CO2, dimethyl sulfide, and O3, J Geophys Res-Oceans, 116, C00F09, 10.1029/2010jc006884, 2011.

551 Goddijn-Murphy, L., Woolf, D. K., and Marandino, C.: Space-based retrievals of air-sea gas transfer velocities
552 using altimeters: Calibration for dimethyl sulfide, J Geophys Res-Oceans, 117, 10.1029/2011jc007535, 2012.

553 Goddijn-Murphy, L., Woolf, D. K., Callaghan, A. H., Nightingale, P. D., and Shutler, J. D.: A reconciliation of
554 empirical and mechanistic models of the air-sea gas transfer velocity, Journal of Geophysical Research: Oceans,
555 121, 818-835, 10.1002/2015jc011096, 2016.

556 Hoover, T. E., and Berkshire, D. C.: Effects of hydration on carbon dioxide exchange across an air-water
557 interface, Journal of Geophysical Research, 74, 456-464, 1969.

558 Huebert, B. J., Blomquist, B. W., Hare, J. E., Fairall, C. W., Johnson, J. E., and Bates, T. S.: Measurement of the
559 sea-air DMS flux and transfer velocity using eddy correlation, Geophysical Research Letters, 31, L23113,
560 10.1029/2004gl021567, 2004.

561 Keeling, R. F.: On the role of large bubbles in air-sea gas exchange and supersaturation in the ocean, Journal of
562 Marine Research, 51, 237-271, 10.1357/0022240933223800, 1993.

563 Kloster, S., Feichter, J., Reimer, E. M., Six, K. D., Stier, P., and Wetzel, P.: DMS cycle in the marine ocean-
564 atmosphere system - a global model study, Biogeosciences, 3, 29-51, 2006.

565 Landwehr, S., Miller, S. D., Smith, M. J., Saltzman, E. S., and Ward, B.: Analysis of the PKT correction for
566 direct CO_2 flux measurements over the ocean, Atm Chem Phys, 14, 3361-3372, 10.5194/acp-14-3361-2014,
567 2014.

568 Landwehr, S., O'Sullivan, N., and Ward, B.: Direct flux measurements from mobile platforms at sea: Motion
569 and airflow distortion corrections revisited, Journal of Atmospheric and Oceanic Technology, 32, 1163-1178,
570 10.1175/jtech-d-14-00137.1, 2015.

571 Le Quéré, C., Moriarty, R., Andrew, R. M., Peters, G. P., Ciais, P., Friedlingstein, P., Jones, S. D., Sitch, S.,
572 Tans, P., Arneth, A., Boden, T. A., Bopp, L., Bozec, Y., Canadell, J. G., Chini, L. P., Chevallier, F., Cosca, C.
573 E., Harris, I., Hoppema, M., Houghton, R. A., House, J. I., Jain, A. K., Johannessen, T., Kato, E., Keeling, R. F.,
574 Kitidis, V., Klein Goldewijk, K., Koven, C., Landa, C. S., Landschützer, P., Lenton, A., Lima, I. D., Marland,
575 G., Mathis, J. T., Metzl, N., Nojiri, Y., Olsen, A., Ono, T., Peng, S., Peters, W., Pfeil, B., Poulter, B., Raupach,
576 M. R., Regnier, P., Rödenbeck, C., Saito, S., Salisbury, J. E., Schuster, U., Schwinger, J., Séférian, R.,
577 Segschneider, J., Steinhoff, T., Stocker, B. D., Sutton, A. J., Takahashi, T., Tilbrook, B., van der Werf, G. R.,
578 Viovy, N., Wang, Y. P., Wanninkhof, R., Wiltshire, A., and Zeng, N.: Global carbon budget 2014, Earth System
579 Science Data, 7, 47-85, 10.5194/essd-7-47-2015, 2015.

580 Liss, P. S., and Slater, P. G.: Flux of gases across the air-sea interface, Nature, 247, 181-184, 1974.

581 Liss, P. S., and Merlivat, L.: Air-sea gas exchange rates: introduction and synthesis, in: The role of air-sea
582 exchange in geochemical cycling, edited by: Buatmenard, P., Reidel, 113-127, 1986.

583 Marandino, C. A., De Bruyn, W. J., Miller, S. D., and Saltzman, E. S.: Eddy correlation measurements of the
584 air/sea flux of dimethylsulfide over the North Pacific Ocean, Journal of Geophysical Research-Atmospheres,
585 112, art. no.-D03301, 10.1029/2006jd007293, 2007.

586 McGillis, W. R., Dacey, J. W. H., Frew, N. M., Bock, E. J., and Nelson, R. K.: Water-air flux of
587 dimethylsulfide, J Geophys Res-Oceans, 105, 1187-1193, 2000.

588 McGillis, W. R., Edson, J. B., Hare, J. E., and Fairall, C. W.: Direct covariance air-sea CO_2 fluxes, J Geophys
589 Res-Oceans, 106, 16729-16745, 2001.

Atmospheric
Chemistry
and Physics
Discussions

590 Melville, W. K., and Matusov, P.: Distribution of breaking waves at the ocean surface, Nature, 417, 58-63,
591 2002.

592 Miller, S. D., Hristov, T. S., Edson, J. B., and Friehe, C. A.: Platform motion effects on measurements of
593 turbulence and air-sea exchange over the open ocean, Journal of Atmospheric and Oceanic Technology, 25,
594 1683-1694, 10.1175/2008jtecho547.1, 2008.

595 Miller, S. D., Marandino, C., de Bruyn, W., and Saltzman, E. S.: Air-sea gas exchange of CO_2 and DMS in the
596 North Atlantic by eddy covariance, Geophysical Research Letters, 36, art. no.-L15816, 10.1029/2009gl038907,
597 2009.

598 Miller, S. D., Marandino, C., and Saltzman, E. S.: Ship-based measurement of air-sea CO_2 exchange by eddy
599 covariance, Journal of Geophysical Research-Atmospheres, 115, art. no.-D02304, 10.1029/2009jd012193, 2010.

600 Pereira, R., Schneider-Zapp, K., and Upstill-Goddard, R. C.: Surfactant control of gas transfer velocity along an
601 offshore coastal transect: results from a laboratory gas exchange tank, Biogeosciences, 13, 3981-3989,
602 10.5194/bg-13-3981-2016, 2016.

603 Rhee, T. S., Nightingale, P. D., Woolf, D. K., Caulliez, G., Bowyer, P., and Andreae, M. O.: Influence of
604 energetic wind and waves on gas transfer in a large wind-wave tunnel facility, J Geophys Res-Oceans, 112, art.
605 no.-C05027, 10.1029/2005jc003358, 2007.

606 Saltzman, E. S., King, D. B., Holmen, K., and Leck, C.: Experimental determination of the diffusion coefficient
607 of dimethylsulfide in water, J Geophys Res-Oceans, 98, 16481-16486, 1993.

608 Saltzman, E. S., De Bruyn, W. J., Lawler, M. J., Marandino, C. A., and McCormick, C. A.: A chemical
609 ionization mass spectrometer for continuous underway shipboard analysis of dimethylsulfide in near-surface
610 seawater, Ocean Science, 5, 537-546, 2009.

611 Scanlon, B., and Ward, B.: Oceanic wave breaking coverage separation techniques for active and maturing
612 whitecaps, Methods in Oceanography, 8, 1-12, 10.1016/j.mio.2014.03.001, 2013.

613 Schwendeman, M., and Thomson, J.: Observations of whitecap coverage and the relation to wind stress, wave
614 slope, and turbulent dissipation, Journal of Geophysical Research: Oceans, 120, 8346-8363,
615 10.1002/2015jc011196, 2015.

616 Stefels, J., Steinke, M., Turner, S., Malin, G., and Belviso, S.: Environmental constraints on the production and
617 removal of the climatically active gas dimethylsulphide (DMS) and implications for ecosystem modelling,
618 Biogeochem, 83, 245-275, 10.1007/s10533-007-9091-5, 2007.

619 Sugihara, Y., Tsumori, H., Ohga, T., Yoshioka, H., and Serizawa, S.: Variation of whitecap coverage with
620 wave-field conditions, Journal of Marine Systems, 66, 47-60, http://dx.doi.org/10.1016/j.jmarsys.2006.01.014,
621 2007.

622 Virkkula, A., Teinilä, K., Hillamo, R., Kerminen, V.-M., Saarikoski, S., Aurela, M., Koponen, I. K., and
623 Kulmala, M.: Chemical size distributions of boundary layer aerosol over the Atlantic Ocean and at an Antarctic
624 site, Journal of Geophysical Research-Atmospheres, 111, art. no.-D05306, 10.1029/2004jd004958, 2006.

625 Wanninkhof, R., Ledwell, J. R., and Broecker, W. S.: Gas exchange-wind speed relation measured with sulfur
626 hexafluoride on a lake, Science, 227, 1224-1226, 10.1126/science.227.4691.1224, 1985.

627 Wanninkhof, R.: Relationship between wind speed and gas exchange over the ocean, J Geophys Res-Oceans,
628 97, 7373-7382, 1992.

629 Wanninkhof, R., and Knox, M.: Chemical enhancement of CO_2 exchange in natural waters, Limnology and
630 Oceanography, 41, 689-697, 10.4319/lo.1996.41.4.0689, 1996.

631 Watson, A. J., Upstill-Goddard, R. C., and Liss, P. S.: Air-sea gas exchange in rough and stormy seas measured
632 by a dual-tracer technique, Nature, 349, 145-147, 1991.

633 Weiss, R. F.: Carbon dioxide in water and seawater: The solubility of a non-ideal gas, Marine Chemistry, 2,
634 203-215, http://dx.doi.org/10.1016/0304-4203(74)90015-2, 1974.

635 Woolf, D. K.: Bubbles and the air-sea transfer velocity of gases, Atmosphere-Ocean, 31, 517-540, 1993.

636 Woolf, D. K.: Bubbles and their role in gas exchange, in: The Sea Surface and Global Change, edited by: Liss,
637 P. S., and Duce, R. A., Cambridge University Press, Cambridge, 173-205, 1997.

Atmospheric
Chemistry
and Physics
Discussions

Open Access

638 Woolf, D. K.: Parametrization of gas transfer velocities and sea-state-dependent wave breaking, Tellus Series B-
639 Chemical and Physical Meteorology, 57, 87-94, 2005.

640 Woolf, D. K., Leifer, I. S., Nightingale, P. D., Rhee, T. S., Bowyer, P., Caulliez, G., de Leeuw, G., Larsen, S. E.,
641 Liddicoat, M., Baker, J., and Andreae, M. O.: Modelling of bubble-mediated gas transfer: Fundamental
642 principles and a laboratory test, Journal of Marine Systems, 66, 71-91,
643 http://dx.doi.org/10.1016/j.jmarsys.2006.02.011, 2007.

644 Woolf, D. K., Land, P. E., Shutler, J. D., Goddijn-Murphy, L. M., and Donlon, C. J.: On the calculation of air-
645 sea fluxes of CO_2 in the presence of temperature and salinity gradients, Journal of Geophysical Research:
646 Oceans, 121, 1229-1248, 10.1002/2015jc011427, 2016.

647 Yang, M., Blomquist, B. W., Fairall, C. W., Archer, S. D., and Huebert, B. J.: Air-sea exchange of
648 dimethylsulfide in the Southern Ocean: Measurements from SO GasEx compared to temperate and tropical
649 regions, J Geophys Res-Oceans, 116, art. no.-C00F05, 10.1029/2010jc006526, 2011.

650 Yang, M., Beale, R., Liss, P., Johnson, M., Blomquist, B., and Nightingale, P.: Air-sea fluxes of oxygenated
651 volatile organic compounds across the Atlantic Ocean, Atm Chem Phys, 14, 7499-7517, 10.5194/acp-14-7499-
652 2014, 2014.

653 Zhao, D., and Toba, Y.: Dependence of whitecap coverage on wind and wind-wave properties, Journal of
654 Oceanography, 57, 603-616, 2001.

655

656

657
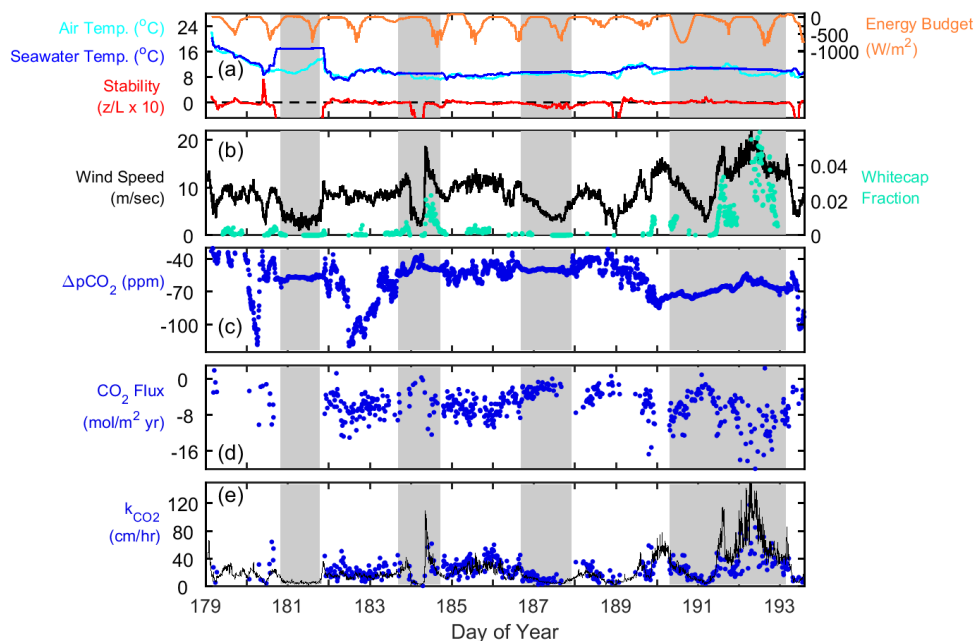
Figure 1: Time series of ten minute averaged data collected during the Knorr_11 cruise. Dashed
black line in panel (a) indicates neutral atmospheric stability (z/L = 0). Grey shaded regions represent
intervals when the ship occupied stations ST181, ST184, ST187, and ST191. Panels (c), (d) and (e)
are the CO_2 concentration difference (ΔpCO_2), flux (F_{CO2}) and gas transfer velocity (k_{CO2}) (water-side
only, no Sc correction), respectively. Panel (e) also shows k_{CO2} calculated using the NOAA COARE
model (black line). Note that negative k_{CO2} data points in (e) were omitted for clarity (see
Supplemental Figure S2 for full data set).

666
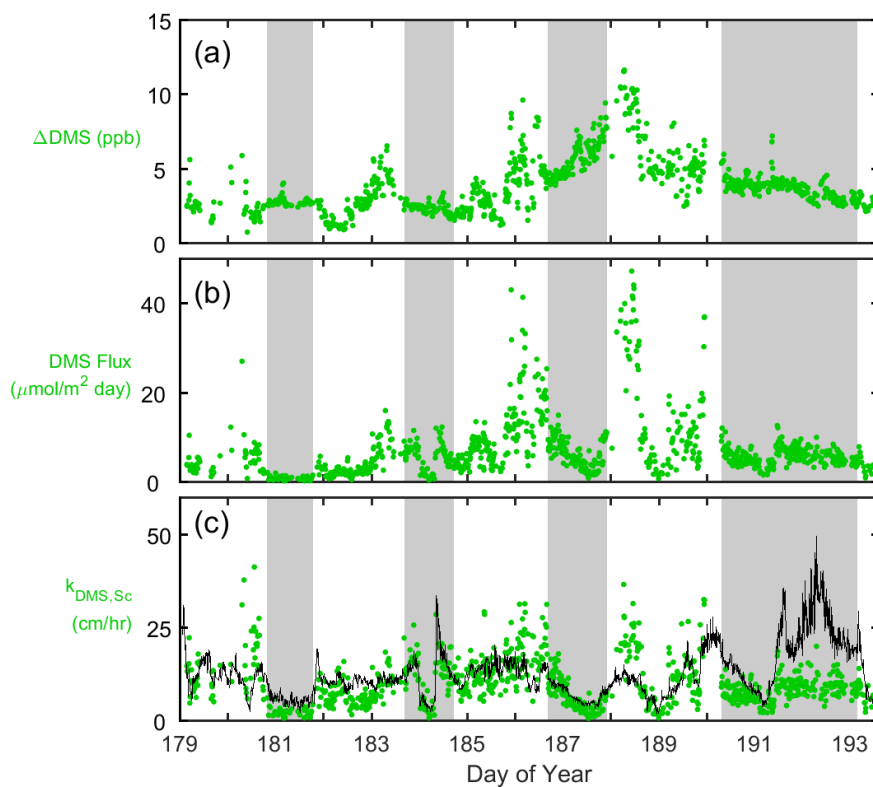
Figure 2: Knorr_11 cruise time series of ten minute averaged DMS: (a) air/sea concentration difference (ΔDMS); (b) flux (F_{DMS}); and (c) gas transfer velocity normalised to the *in situ* CO_2 *Sc* number ($k_{DMS,Sc}$). Panel (c), shows $k_{DMS,Sc}$ calculated using NOAA COARE model output (black line). Grey shaded regions represent periods on station.

671

672

673
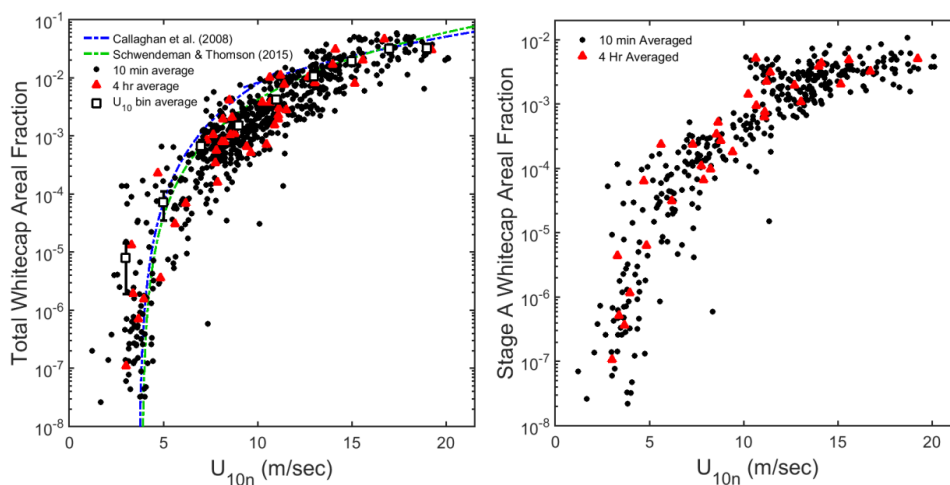
Figure 3: Semi-log plots of whitecap areal fraction as a function of mean horizontal wind speed at 10 m above the sea surface (U_{10}) during the Knorr_11 cruise. 10 min average (black dots) and 4 hour average (red triangles) data are shown on both panels. Left panel shows total whitecap area versus U_{10} bin averaged data (open squares, 2 m s^{-1} bins). Wind speed parameterisations from the recent literature are shown for reference. Right panel is the whitecap area considered to be solely from wave breaking (Stage A whitecaps, see text for definition).

680

681
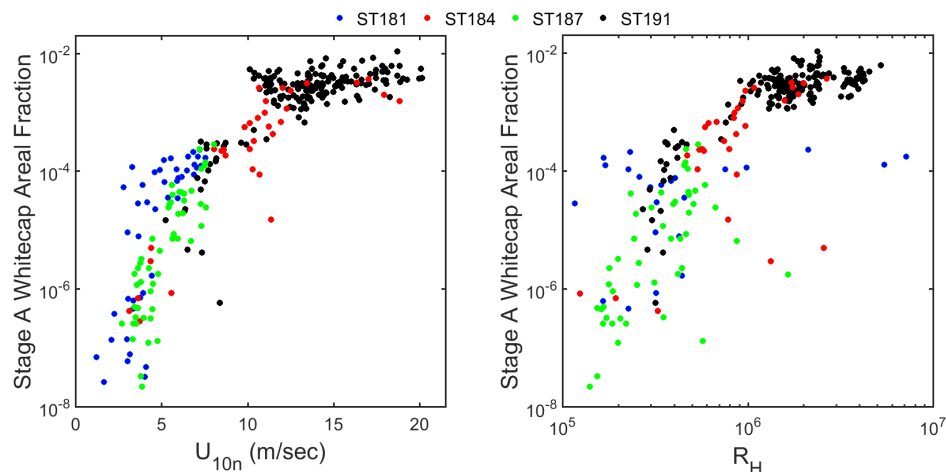
Figure 4: Semi-log plots of Stage A whitecap areal fraction as a function of wind speed (U_{10}, left
panel) and as a function of a non-dimensional Reynolds breaking wave parameter R_H (right panel),
calculated from Knorr_11 measurements of significant wave height (Zhao and Toba, 2001). Plots
show data only from when the ship was on station, segregated into ST181 (blue), ST184 (red), ST187
(green) and ST191 (black). The highly variable Stage A whitecap fraction vs. U_{10} at ~11 m s^{-1} is
driven by differences in the wave environment during ST184 and ST191. Stage A whitecap fraction
vs. R_H exhibits no bimodal behaviour and there is no clear difference between ST184 and ST191. The
relationship between Stage A whitecap fraction and R_H is more scattered when Stage A whitecaps are
below ~10^{-4}.

682
683
684
685
686
687
688
689
690
691

25

692

693

694
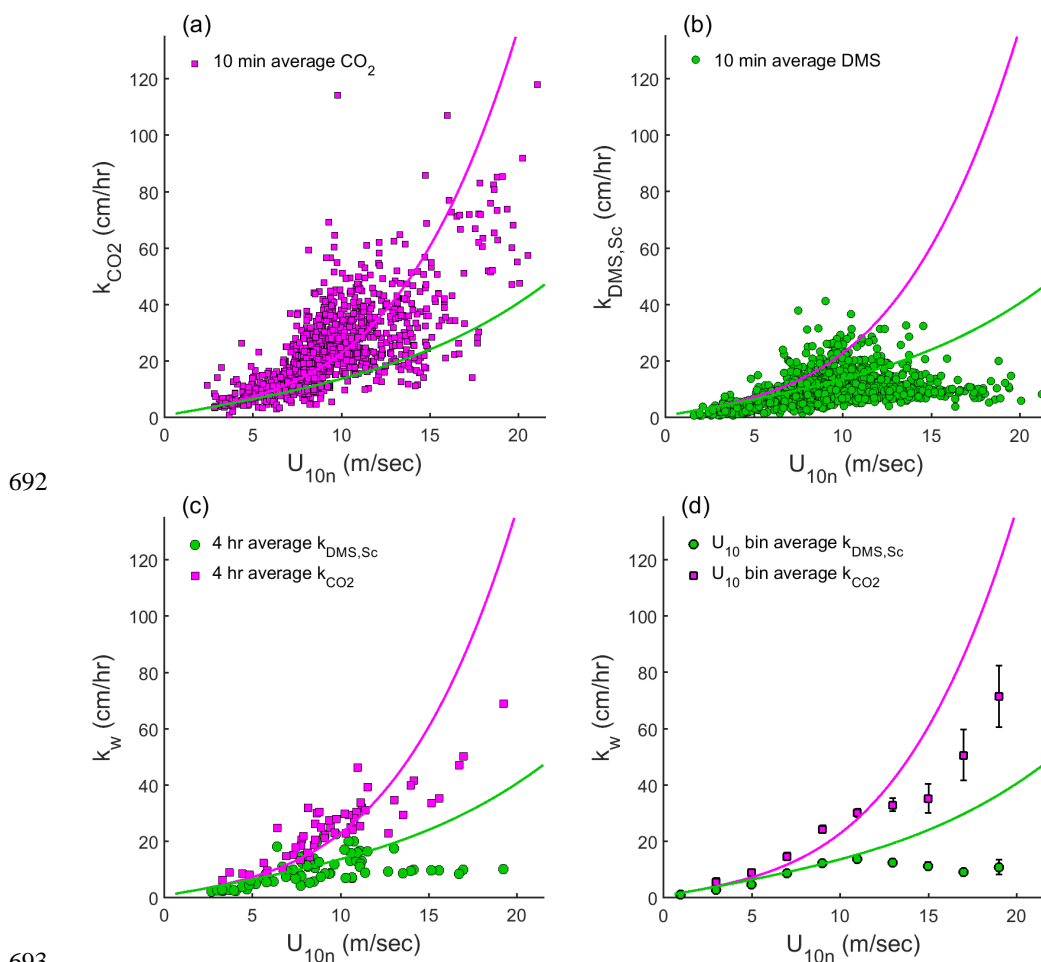
Figure 5: Gas transfer velocities plotted against mean horizontal wind speed (U_{10}) from the Knorr_11 cruise. Ten minute average data for CO_2 (a) and DMS (b). DMS gas transfer velocities are normalised to the *in situ* CO_2 *Sc* number. Data are averaged into 4 hour periods (c) and 2 m s^{-1} wind speed bins (d). Note that negative k_{CO2} data in (a) and (c) have not been plotted for clarity (see Supplemental Figure S4 for full data set). For reference, the NOAA COAREG3.1 model output for CO_2 (magenta line) and DMS (green line) is plotted on all four panels. The COARE model was run with the turbulent/molecular coefficient, A = 1.6, and the bubble-mediated coefficient, B = 1.8, and used mean Knorr_11 data for the input parameters.

703

704
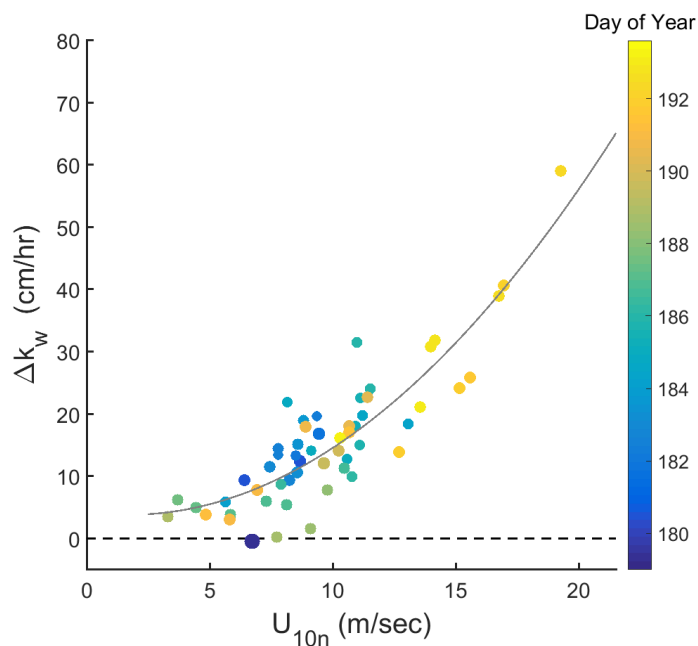
Figure 6: Difference (Δk_w) between 4 hour average k_{CO_2} and $k_{DMS,Sc}$ plotted against U_{10}. Data are coloured by the date of measurement (Day of Year). The solid grey line describes a cubic fit to the data (see text for coefficients).

705
706
707
708

Atmospheric
Chemistry
and Physics
Discussions

709
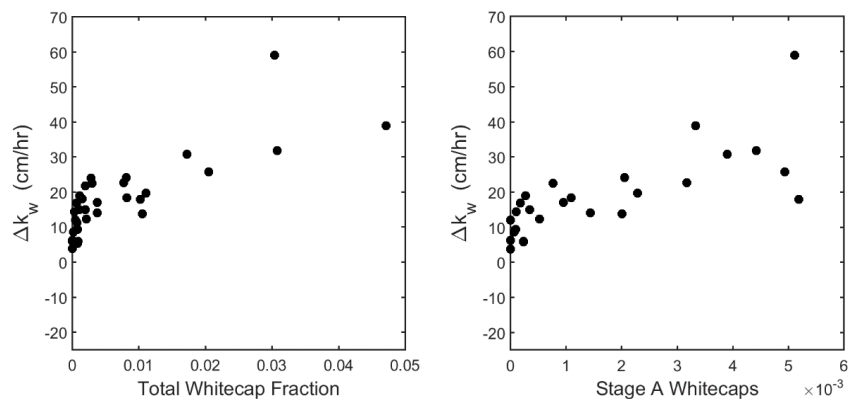
Figure 7: Knorr_11 Δk_w data plotted against total whitecap areal fraction (left panel) and against Stage
A whitecap areal fraction (right panel). Each point is a 4 hour average of coincident measurements of
whitecap fraction and DMS and CO_2 gas transfer.

714
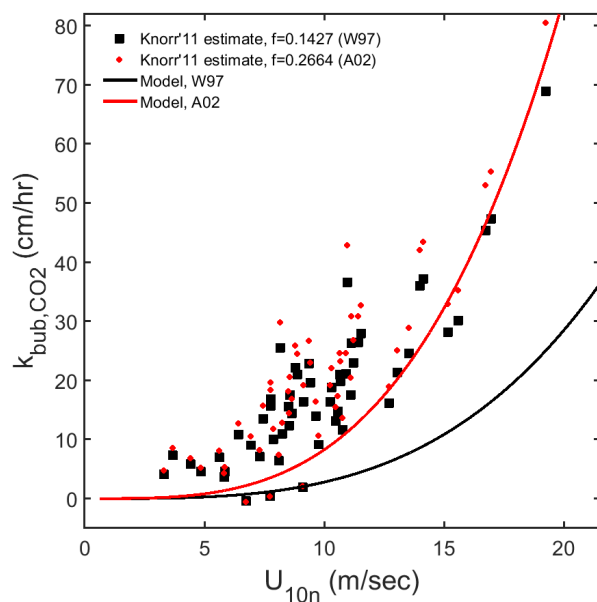
Figure 8: Bubble-mediated transfer velocity of CO_2 (k_{bub,CO_2}) as a function of wind speed. Individual points are Knorr_11 observations using solubility and diffusivity scaling from Woolf (1997) (black squares) and Asher et al. (2002) (red circles). Continuous lines are model calculations of k_{bub,CO_2} using the Knorr_11 wind speed-whitecap areal fraction relationship and mean SST (Woolf (1997), black; Asher et al. (2002), red).

720